

Supporting Information

**Active-site stabilized Bi metal-organic framework-based catalyst for
highly active and selective electroreduction of CO₂ to formate over a
wide potential window**

Leliang Cao^a, Jie Huang^a, Xueying Wu^a, Ben Ma^a, Qingqing Xu^a, Yuanhong Zhong^{a, b*}, Ying Wu^{a, b*}, Ming Sun^{a, b}, Lin Yu^{a, b*}

^aKey Laboratory of Clean Chemistry Technology of Guangdong Regular Higher Education Institutions, Guangdong Engineering Technology Research Center of Modern Fine Chemical Engineering, School of Chemical Engineering and Light Industry, Guangdong University of Technology, 510006 Guangzhou, P. R.China

^bJieyang Branch of Chemistry and Chemical Engineering Guangdong Laboratory (Rongjiang Laboratory), Jieyang 515200, P. R. China

Contents

Fig. S1. (a) NMR trace of formate at -0.9 V potential for ECR by Bi-BDC-120 °C, (b) NMR standard curve of formate.....	1
Fig. S2. (a-b) The SEM images of Bi-BDC-100 °C, (c-d) Bi-BDC-120 °C, and (e-f) Bi-BDC-140 °C.....	1
Fig. S3. (a) TEM and (b) HR-TEM image of the Bi-BDC-140 °C catalyst	2
Fig. S4. XPS spectra of the Bi-BDC-140 °C: (a) survey scan, (b) C 1s, (c) Bi 4f, and (d) O 1s....	2
Fig. S5. Faraday efficiency (FE) of the products by Bi-BDC-T at -1.1 V vs RHE.....	3
Fig. S6. Chronoamperometric responses at different working potentials in CO ₂ saturated 0.1 mol L ⁻¹ KHCO ₃ catalyzed by (a) Bi-BDC-100 °C, (b) Bi-BDC-120 °C, (c) Bi-BDC-140 °C and (d)commercial Bi ₂ O ₃	3
Fig. S7. Faraday efficiency (FE) of H ₂ and CO at different working potentials.	4
Fig. S8. (a) FE of products and current density at different working potentials in Ar-saturated electrolyte using Bi-BDC-120 °C as electrocatalyst. (b) NMR trace at -0.9 V potential in Ar-saturated electrolyte using Bi-BDC-120 °C as electrocatalyst.....	4
Fig. S9. Energy efficiencies (EE) of formate at different working potentials for ECR catalyzed by Bi-BDC-100 °C, 120 °C,140 °C, and commercial Bi ₂ O ₃	5
Fig. S10. Electrochemically surface area (ECSA) measurements. Cyclic voltammograms (CVs) of different catalysts at various sweep speeds (20–100 mV s ⁻¹) in the region of 0.10 to 0.20 V vs. RHE: (a) Bi-BDC-100 °C (b) Bi-BDC-120 °C (c) Bi-BDC-140 °C and (d) commercial Bi ₂ O ₃	5
Fig. S11. Comparison of Linear Scanning Voltammogram (LSV) curves before and after the 36-hour stability test.....	6
Fig. S12. FEsformate for catalysts synthesized with different molar ratios of Bi(NO ₃) ₃ ·5H ₂ O to H ₂ BDC.....	6
Fig.S13. FEsformate for catalysts synthesized with various stock concentrations but keeping the same molar ratios of Bi(NO ₃) ₃ ·5H ₂ O and H ₂ BDC (i.e., 0.3:0.45, 2:3, 4:6, 6:9, and 9:13.5).	7
Fig. S14 Theoretical calculation of CO ₂ adsorption on the surface of (a) Bi ₂ O ₃ (b) Bi-BDC, and the crystal surface diagram of CO ₂ adsorption by (c) Bi ₂ O ₃ (d-f) Bi-BDC.....	7
Fig.S15. XRD patterns of the synthesized Bi ₂ O ₂ CO ₃	8
Fig.S16. (a) Faraday efficiency of formate at different working potentials with synthesized Bi ₂ O ₂ CO ₃ catalysts. (b) The bias current densities of formate. (c) Energy efficiencies (EE) of formate. (d) Cyclic voltammograms (CVs) of synthesized Bi ₂ O ₂ CO ₃ . (e) ECSA measurement. The charging current densities are plotted against the scan rates of CVs. (f) Nyquist plots for Bi-BDC-120 °C and synthesized Bi ₂ O ₂ CO ₃ with the fitted circuit shown.....	8
Table S1 Comparison of Bi-BDC-120 °C with the reported Bi-based catalysts for ECR conversion of CO ₂ to formate.....	9

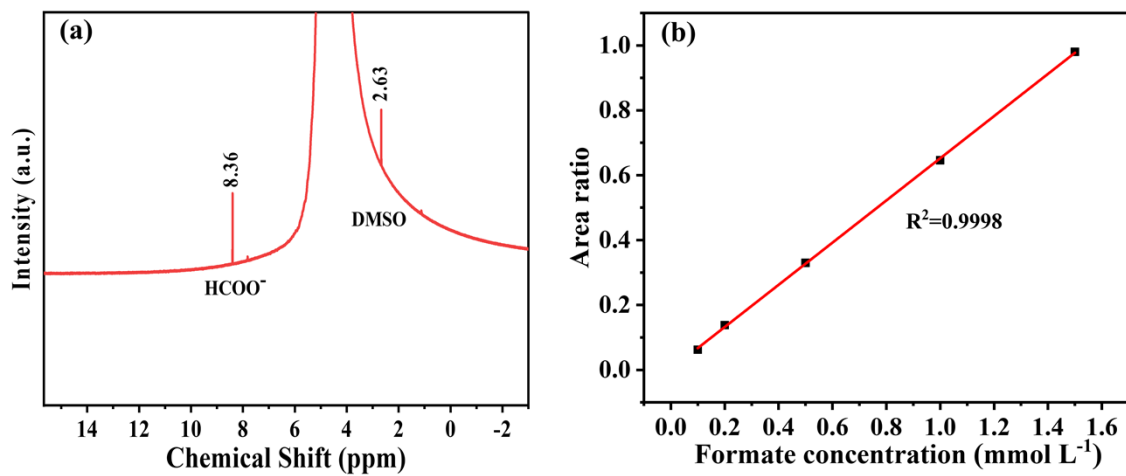


Fig. S1. (a) NMR trace of formate at -0.9 V potential for ECR by Bi-BDC-120 °C, (b) NMR standard curve of formate.

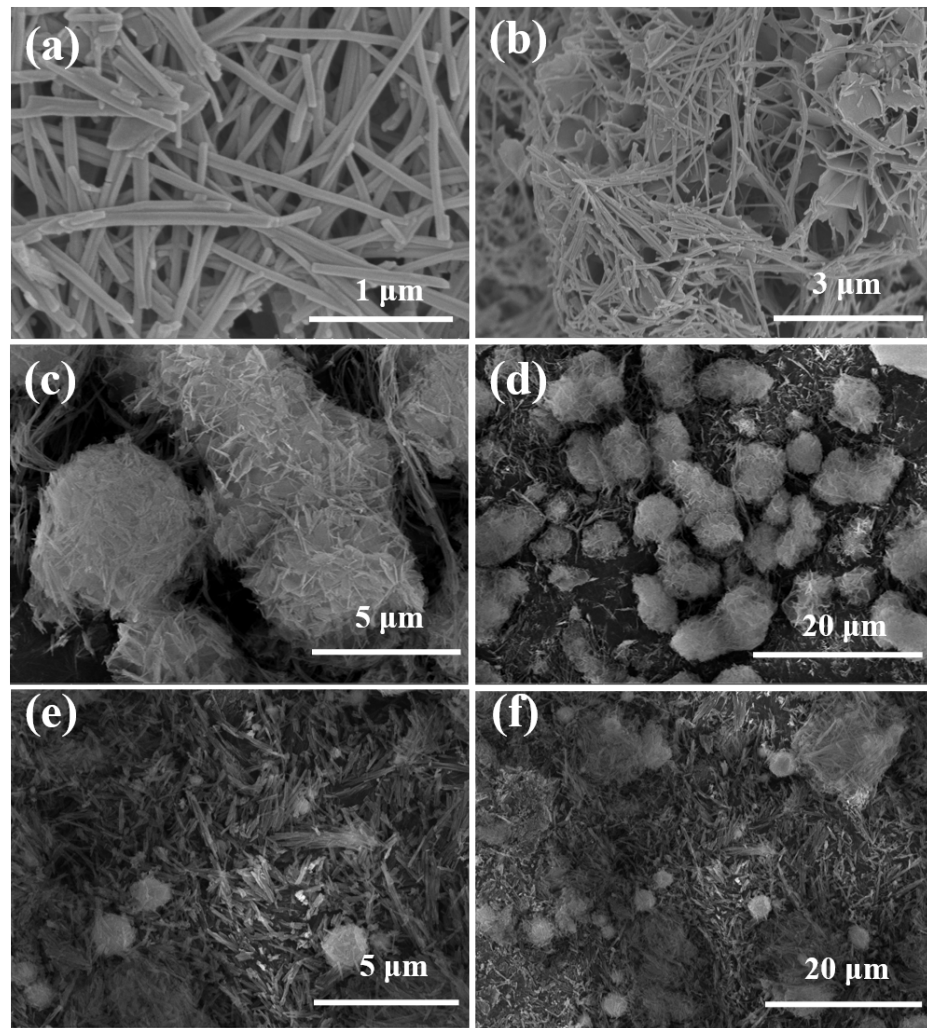


Fig. S2. (a-b) The SEM images of Bi-BDC-100 °C, (c-d) Bi-BDC-120 °C, and (e-f) Bi-BDC-140 °C.

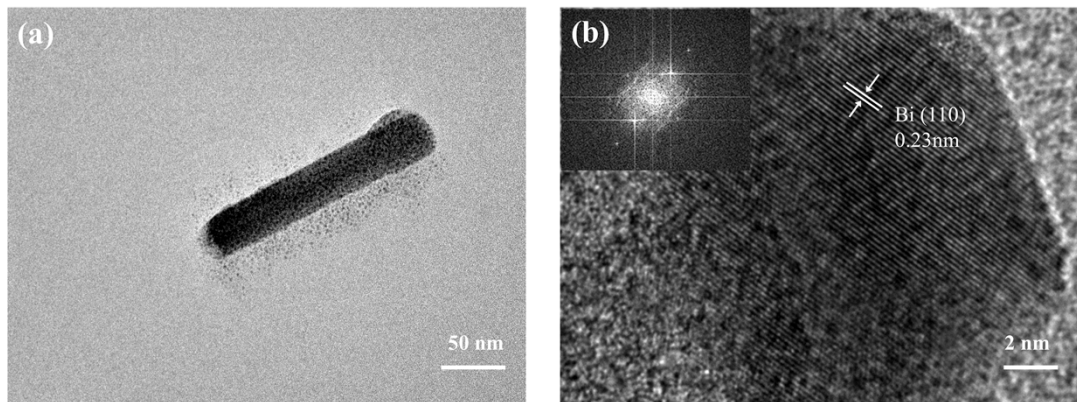


Fig. S3. (a) TEM and (b) HR-TEM image of the Bi-BDC-140 °C catalyst

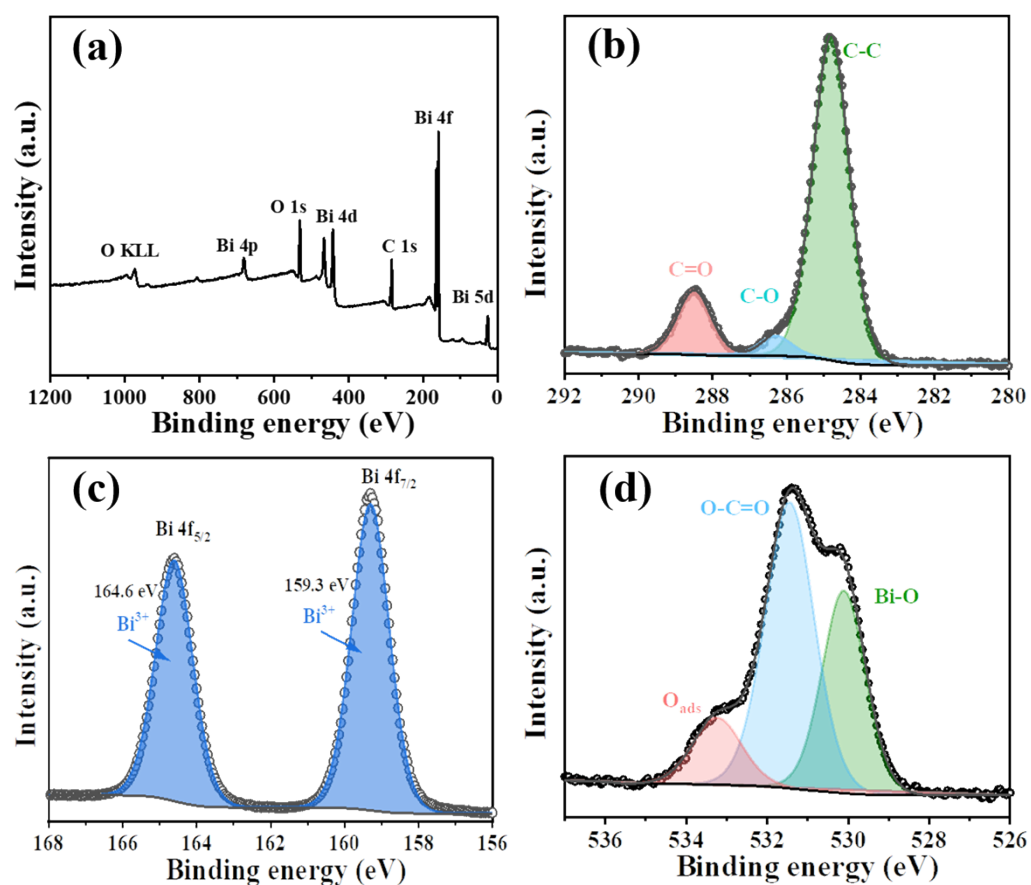


Fig. S4. XPS spectra of the Bi-BDC-140 °C: (a) survey scan, (b) C 1s, (c) Bi 4f, and (d) O 1s

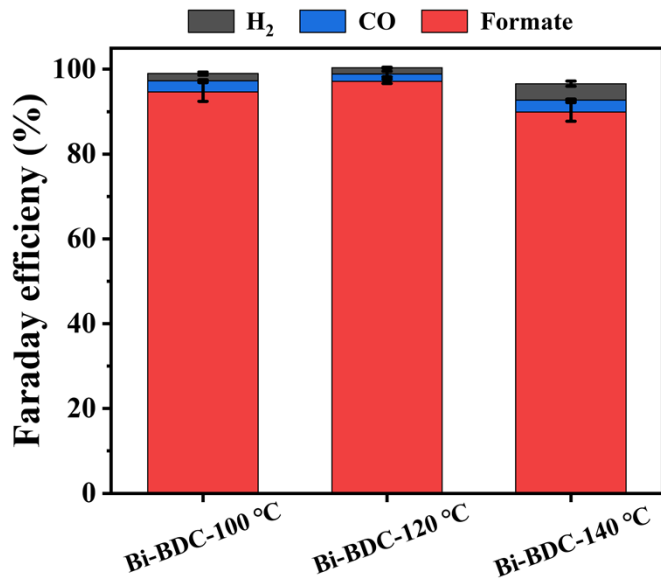


Fig. S5. Faraday efficiency (FE) of the products by Bi-BDC-T at -1.1 V vs RHE.

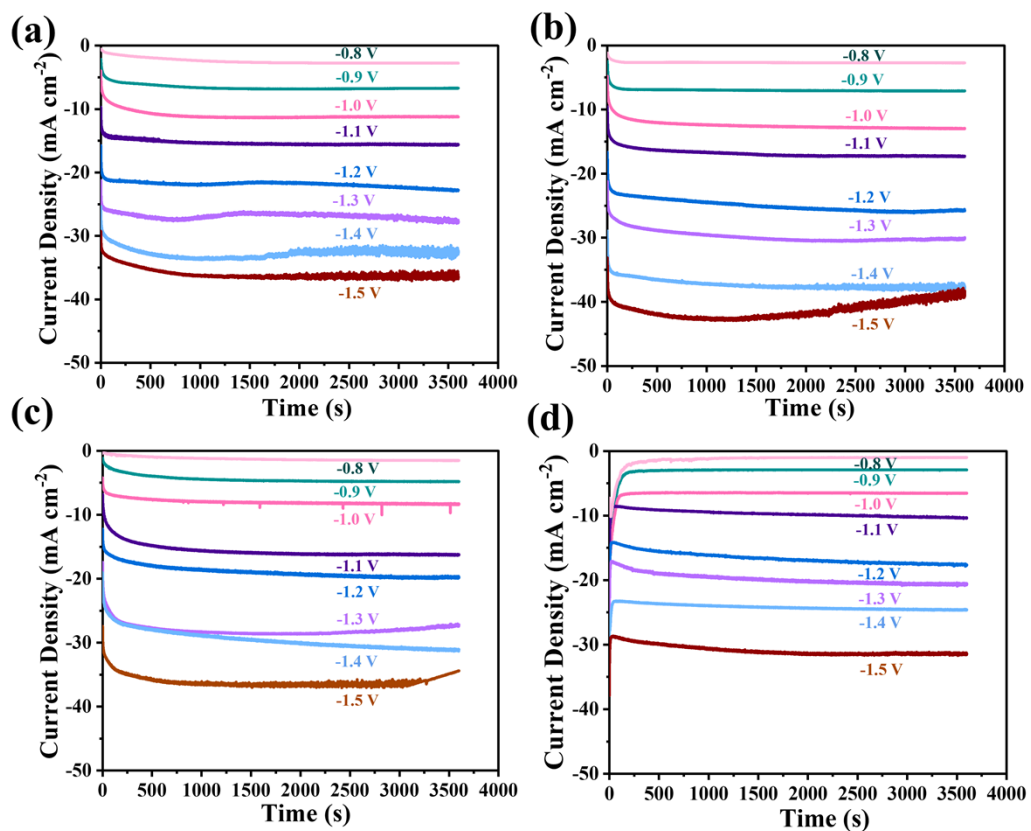


Fig. S6. Chronoamperometric responses at different working potentials in CO_2 saturated $0.1 \text{ mol L}^{-1} \text{ KHCO}_3$ catalyzed by (a) Bi-BDC-100 °C, (b) Bi-BDC-120 °C, (c) Bi-BDC-140 °C and (d) commercial Bi_2O_3 .

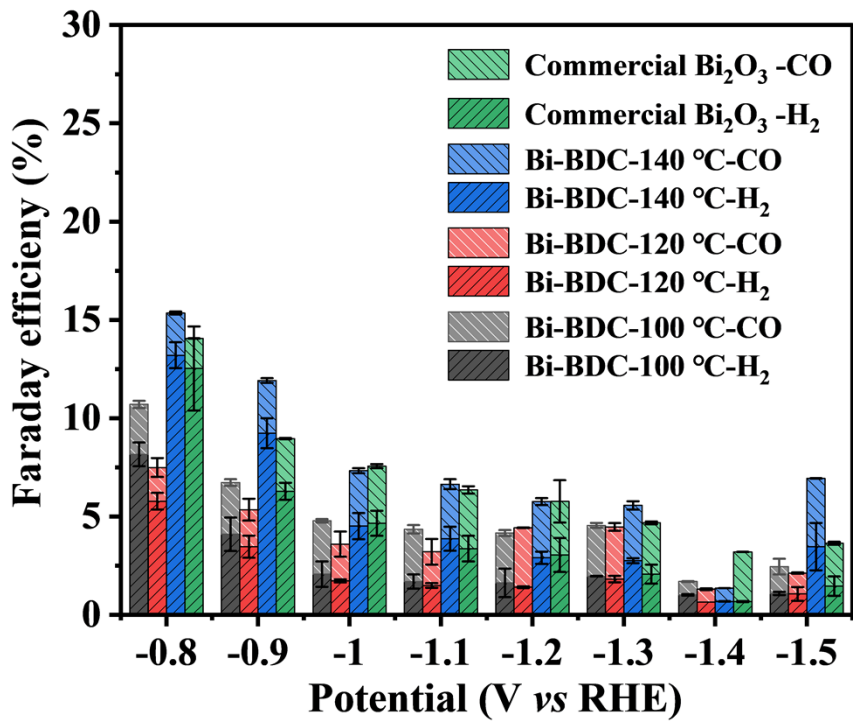


Fig. S7. Faraday efficiency (FE) of H₂ and CO at different working potentials.

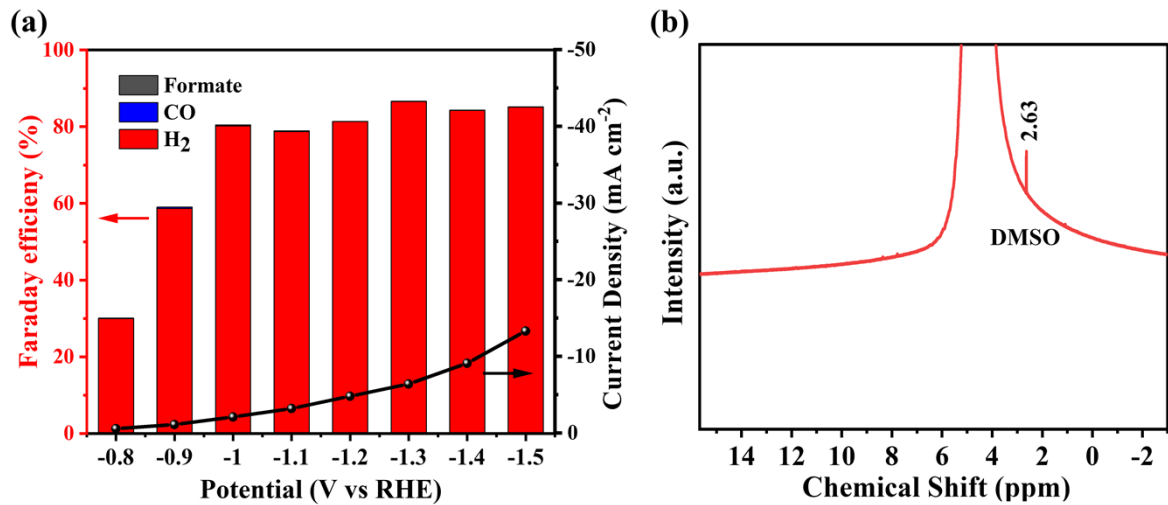


Fig. S8. (a) FE of products and current density at different working potentials in Ar-saturated electrolyte using Bi-BDC-120 °C as electrocatalyst. (b) NMR trace at -0.9 V potential in Ar-saturated electrolyte using Bi-BDC-120 °C as electrocatalyst.

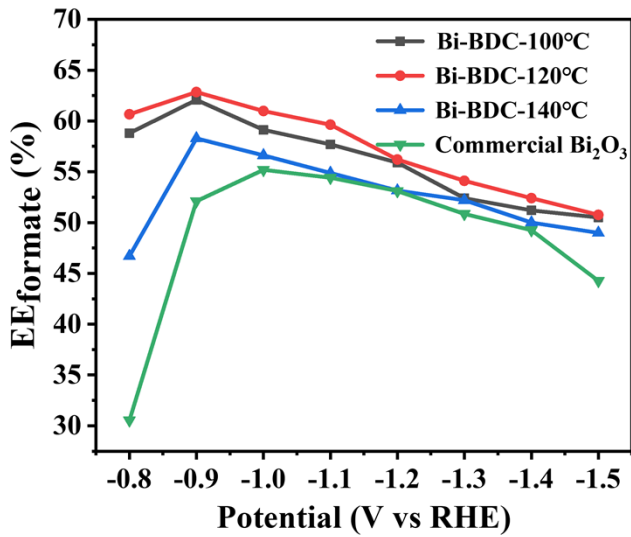


Fig. S9. Energy efficiencies (EE) of formate at different working potentials for ECR catalyzed by Bi-BDC-100 °C, 120 °C, 140 °C, and commercial Bi_2O_3 .

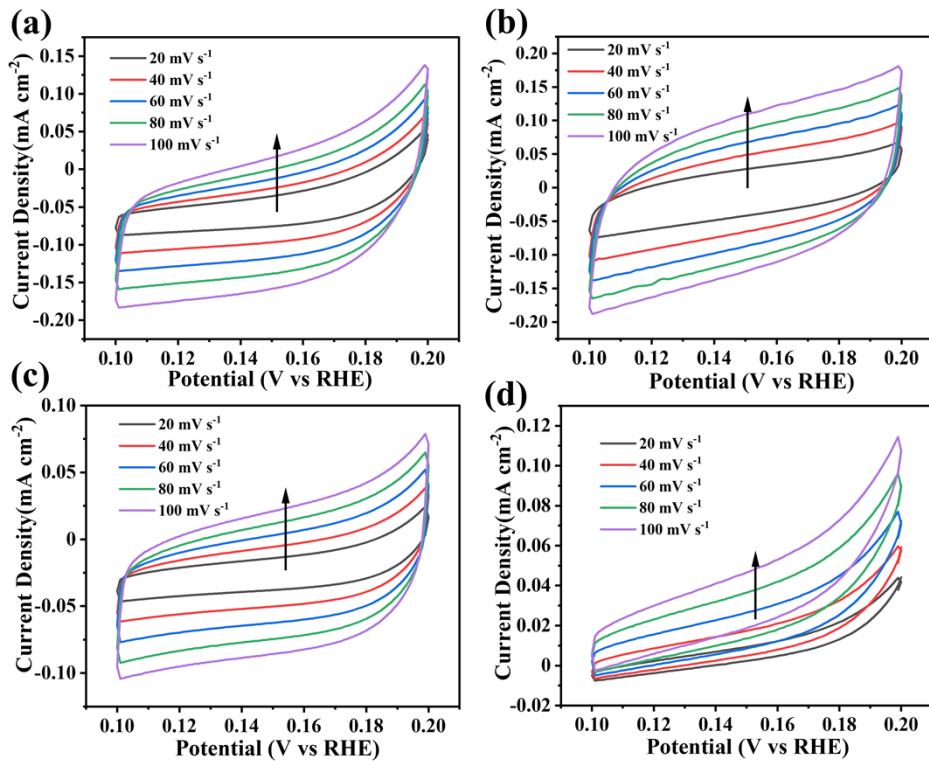


Fig. S10. Electrochemically surface area (ECSA) measurements. Cyclic voltammograms (CVs) of different catalysts at various sweep speeds (20–100 mV s^{-1}) in the region of 0.10 to 0.20 V vs. RHE: (a) Bi-BDC-100 °C (b) Bi-BDC-120 °C (c) Bi-BDC-140 °C and (d) commercial Bi_2O_3 .

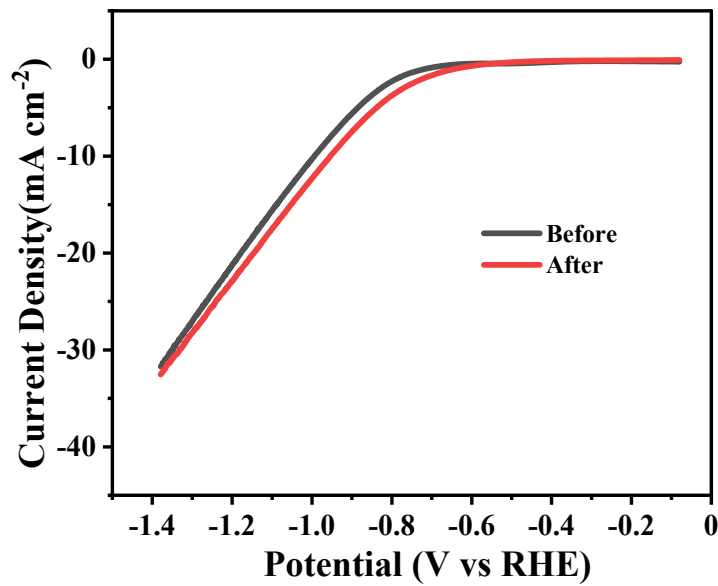


Fig. S11. Comparison of Linear Scanning Voltammogram (LSV) curves before and after the 36-hour stability test.

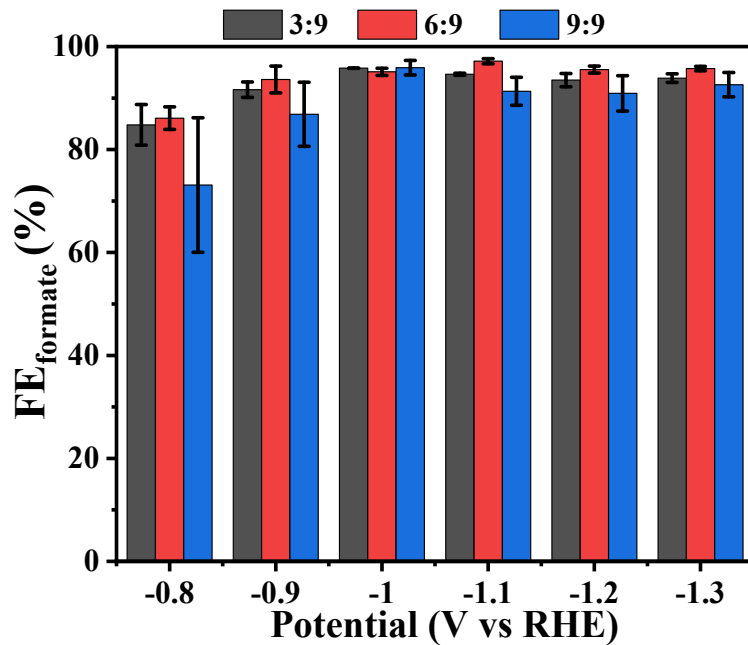


Fig. S12. FE_{formate} for catalysts synthesized with different molar ratios of $\text{Bi}(\text{NO}_3)_3 \cdot 5\text{H}_2\text{O}$ to H_2BDC .

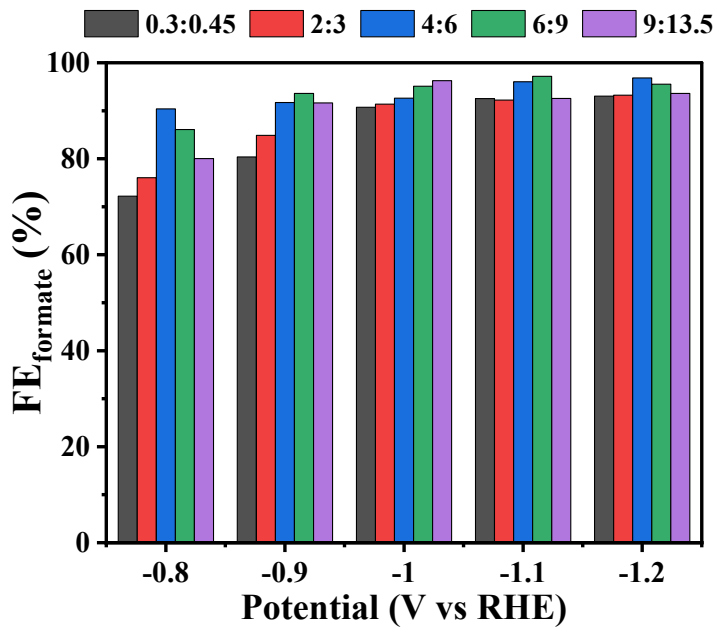


Fig.S13. FEsformate for catalysts synthesized with various stock concentrations but keeping the same molar ratios of Bi(NO₃)₃·5H₂O and H₂BDC (i.e., 0.3:0.45, 2:3, 4:6, 6:9, and 9:13.5).

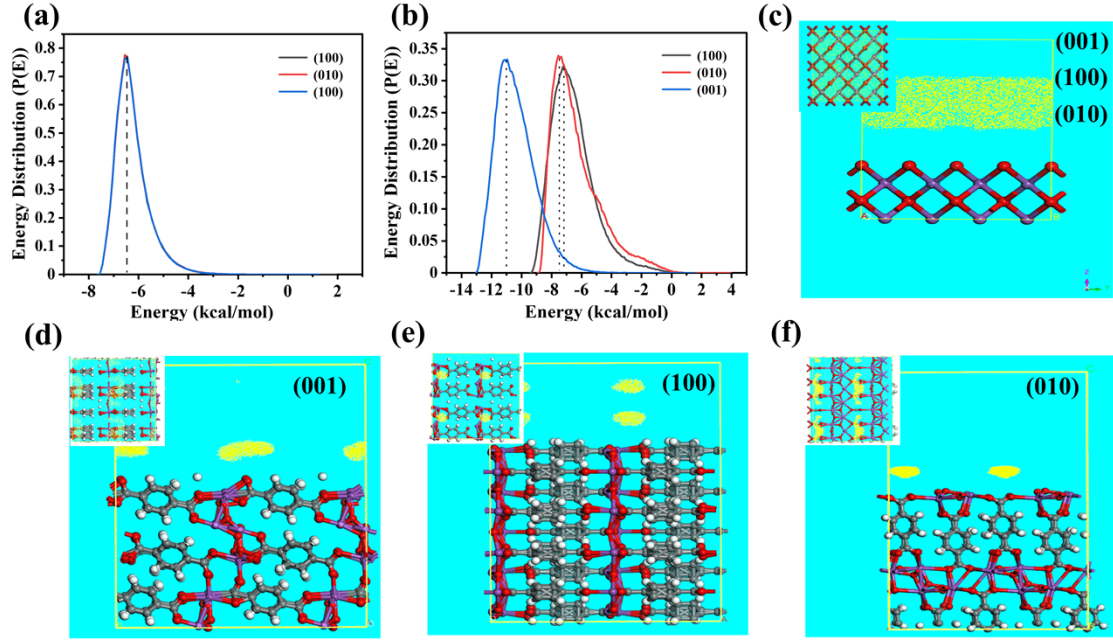


Fig. S14 Theoretical calculation of CO₂ adsorption on the surface of (a) Bi₂O₃ (b) Bi-BDC, and the crystal surface diagram of CO₂ adsorption by (c) Bi₂O₃ (d-f) Bi-BDC.

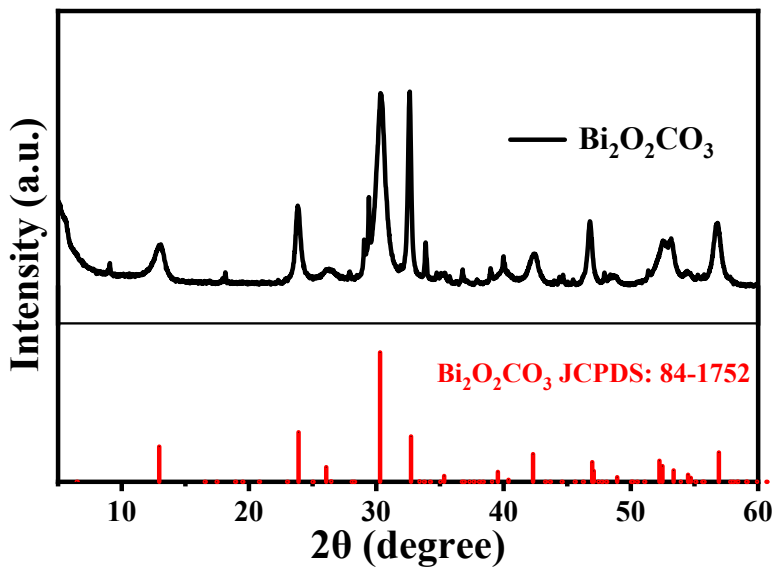


Fig.S15. XRD patterns of the synthesized $\text{Bi}_2\text{O}_2\text{CO}_3$.

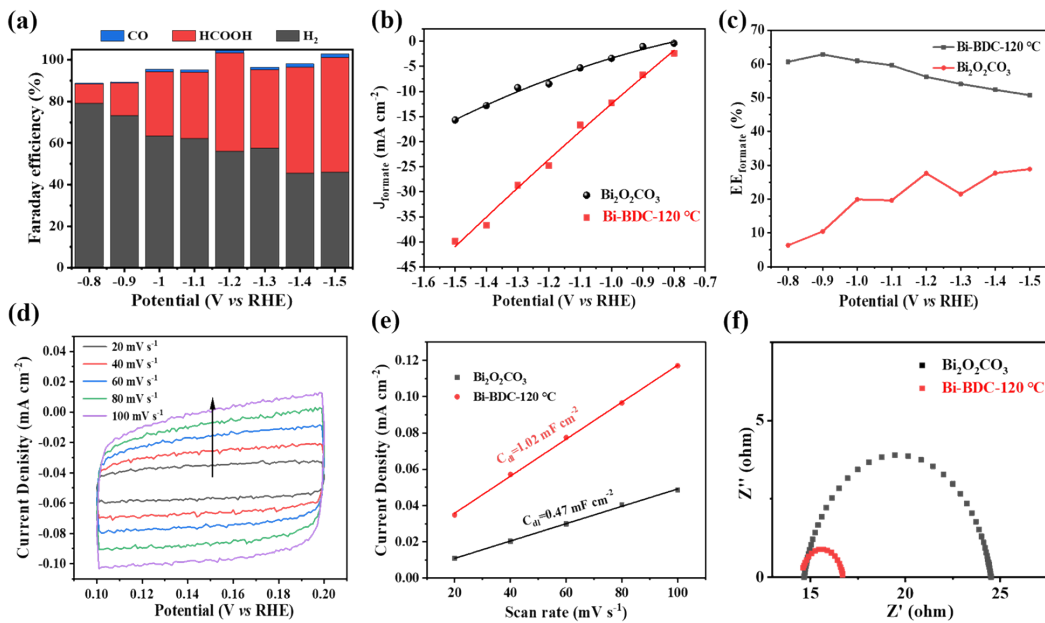


Fig.S16. (a) Faraday efficiency of formate at different working potentials catalyzed by the synthesized $\text{Bi}_2\text{O}_2\text{CO}_3$. (b) Comparison of the bias current densities and (c) Energy efficiencies (EE) of formate catalyzed with $\text{Bi}_2\text{O}_2\text{CO}_3$ and Bi-BDC-120 °C. (d) Cyclic voltammograms (CVs) of synthesized $\text{Bi}_2\text{O}_2\text{CO}_3$. (e) Comparison of ECSA measurement catalyzed with $\text{Bi}_2\text{O}_2\text{CO}_3$ and Bi-BDC-120 °C, and the charging current densities were plotted against the scan rates of CVs. (f) Nyquist plots for Bi-BDC-120 °C and synthesized $\text{Bi}_2\text{O}_2\text{CO}_3$ with the fitted circuit shown.

Table S1 Comparison of Bi-BDC-120 °C with the reported Bi-based catalysts for ECR conversion of CO₂ to formate.

Catalysts	Electrolyte	E (V vs. RHE)	FE _{formate} (%)	J _{formate} (mA cm ⁻²)	Window (mV)	Stability	Ref.
Bi-BDC-120 °C	0.1 M KHCO₃	-0.9	93.6	-6.6	700	36 h	This work
		-1.1	97.2	-16.7			This work
Bi-MP	1 M KOH	-1.0	95	-180 (flow-cell)	600	10 h	1
Bi-BTC	0.1 M KHCO ₃	-1.1	80	-8	400	30 h	2
Bi-BTC-D	0.5 M KHCO ₃	-0.86	95.5	-11.2	400	12 h	3
Bi ₂ O ₃ @C	0.5 M KHCO ₃	-0.9	93	-7.5	300	10 h	4
Bi/CeOx	0.2 M NaSO ₄	-1.3	92	-137 (flow-cell)	500	30 h	5
Bi Ns	0.1 M KHCO ₃	-1.1	92	-9	300	10 h	6
PNCB	0.5 M KHCO ₃	-1.05	92.3	-22	400	No date	7
Bi-Sn	0.5 M KHCO ₃	-1.14	94	-40.2	300	No date	8
Bi/Bi ₂ O ₃ -CP	0.5 M KHCO ₃	-0.87	90.4	-38.8	200	17 h	9
Bi/CN	0.1 M KHCO ₃	-1.3	98	-15.7	500	20 h	10
Bi ₂ O ₃ NSS@MCCM	0.1 M KHCO ₃	-1.256	93.8	-15.1	400	12 h	11
Bi ₂ O ₂ CO ₃	0.5 M KHCO ₃	-0.669	96.1	-9.61	300	48 h	12
Cu NWs-Bi NSS	0.1 M KHCO ₃	-0.86	87	-4.5	100	8 h	13

Reference

1. C. Lin, Y. Liu, X. Kong, Z. Geng and J. Zeng, *Nano Res.*, 2022, **15**, 10078-10083.
2. L. Liu, K. Yao, J. Fu, Y. Huang, N. Li and H. Liang, *Colloid Surface A*, 2022, **633**, 127840.
3. L. Jiao, W. Yang, G. Wan, R. Zhang, X. Zheng, H. Zhou, S. H. Yu and H. L. Jiang, *Angew. Chem. Int. Ed.*, 2020, **132**, 20770-20776.
4. P. Deng, F. Yang, Z. Wang, S. Chen, Y. Zhou, S. Zaman and B. Y. Xia, *Angew. Chem. Int. Ed.*, 2020, **59**, 10807-10813.
5. Y. X. Duan, Y. T. Zhou, Z. Yu, D. X. Liu, Z. Wen, J. M. Yan and Q. Jiang, *Angew. Chem. Int. Ed.*, 2021, **60**, 8798-8802.
6. D. Yao, C. Tang, A. Vasileff, X. Zhi, Y. Jiao and S. Z. Qiao, *Angew. Chem. Int. Ed.*, 2021, **60**, 18178-18184.
7. Y. Wang, L. Xu, L. Zhan, P. Yang, S. Tang, M. Liu, X. Zhao, Y. Xiong, Z. Chen and Y. Lei, *Nano Energy*, 2022, **92**, 106780.
8. G. Wen, D. U. Lee, B. Ren, F. M. Hassan, G. Jiang, Z. P. Cano, J. Gostick, E. Croiset, Z. Bai, L. Yang and Z. Chen, *Adv. Energy Mater.*, 2018, **8**, 1802427.
9. D. Wu, G. Huo, W. Chen, X.-Z. Fu and J.-L. Luo, *Appl. Catal. B: Environ.*, 2020, **271**, 118957.
10. X. Ma, J. Tian, M. Wang, M. Shen and L. Zhang, *J. Colloid Interf. Sci.*, 2022, **608**, 1676-1684.
11. S. Liu, X. F. Lu, J. Xiao, X. Wang and X. W. D. Lou, *Angew. Chem. Int. Ed.*, 2019, **58**, 13828-13833.
12. W.-W. Yuan, J.-X. Wu, X.-D. Zhang, S.-Z. Hou, M. Xu and Z.-Y. Gu, *J. Mater. Chem. A*, 2020, **8**, 24486-24492.
13. L. Li, F. Cai, F. Qi and D.-K. Ma, *J. Alloys Compd.*, 2020, **841**, 155789.